Modelling and parameter estimation of breakthrough curves for amine-modified activated carbons under pre-combustion carbon capture conditions

Azpiri, Rebeca; Soares Dos Santos, Douglas; Ingram, Andy; Wood, Joe

DOI:
10.1016/j.fuel.2019.05.095

Document Version
Early version, also known as pre-print

Citation for published version (Harvard):
Azpiri, R, Soares Dos Santos, D, Ingram, A & Wood, J 2019, 'Modelling and parameter estimation of breakthrough curves for amine-modified activated carbons under pre-combustion carbon capture conditions' Fuel, vol. 253, pp. 1130-1139. https://doi.org/10.1016/j.fuel.2019.05.095

Modelling and Parameter Estimation of Breakthrough Curves for Amine-modified Activated Carbons under Pre-Combustion Carbon Capture Conditions

*Rebeca A. Azpiri Solares[§], Douglas Soares dos Santos[§], Andrew Ingram and Joseph Wood**

School of Chemical Engineering, University of Birmingham, Edgbaston, Birmingham B15 2TT, United Kingdom

*Corresponding author.

[§]Rebeca A. Azipiri Solares carried out the process simulation work and Douglas Soares dos Santos carried out the experimental work. Equally weighted contributions are attributed to their work towards this article.

E- mail address: J.Wood@bham.ac.uk.

ABSTRACT: Pressure Swing Adsorption (PSA) demonstrates high potential for capturing pre-combustion carbon dioxide in Integrated Gasification Combined Cycle (IGCC) power plants, due to a binary mixture of hydrogen and carbon dioxide entering the separation process. In this work, a seven-step PSA model was developed and compared to adsorption experiments under PSA conditions (25 bar and ambient temperatures) performed with tetraethylenepentamine (TEPA) and a novel blend of monoethanolamine-monodiethanolamine (MEA-MDEA)

modified activated carbons, using nitrogen and carbon dioxide mixtures. The MEA-MDEA modified activated carbon showed promising results for pre-combustion PSA processes, due to their high carbon dioxide adsorption capacity and delayed break-point of about 200 s compared to the unmodified activated carbons. A sensitivity analysis carried out for the adsorbent parameters in a seven-step PSA process showed that high mass transfer coefficient values yielded to highly purified products, specifically for the light product stream (99.4%). A sensitivity analysis of the process variables showed that purity values of the heavy stream (carbon dioxide) were over 90% when the purge pressure was reduced to 0.5 bar and the carbon dioxide feed fraction increased to 60%.

KEYWORDS: CCS; Pressure Swing Adsorption; Pre-combustion; Activated carbon; Monoethanolamine.

Nomenclature

C_i	**Concentration of i component in the gas phase (mol/m^3)**
Q_i	**Sorbent loading of i component (mol/kg)**
e	**Gas phase density (kg/m^3)**
e_s	**Sorbent density (kg/m^3)**
e_w	**Bed wall density (kg/m^3)**
$\mathcal{E}_b$	**Bed void fraction**
$\mathcal{E}_p$	**Particle void fraction**
$\mathcal{E}_t$	**Total void fraction**
v	**Gas velocity (m/s)**
R	**Ideal gas constant (J/mol. K)**
t	**Time (s)**
T	**Temperature (K)**
T_w	**Wall temperature (K)**

P	**Pressure (Pa)**
λ	**Axial heat dispersion coefficient (W/ m. K)**
ΔH_i^{ads}	**Heat of adsorption of i component (kJ/mol)**
C^i_{pg}	**Specific heat of i component in the gas phase (kJ/mol. K)**
C_{ps}	**Specific heat of the sorbent (kJ/kg. K)**
C_{pw}	**Specific heat of the wall (kJ/kg. K)**
h_i	**Effective heat transfer coefficient (kW/m^2. K)**
μ_g	**Viscosity of the gas phase (Pa. s)**
d_p	**Particle diameter (m)**
M^i_w	**Molecular weight of i component (kg/mol)**
b	**Langmuir isotherm constant (1/Pa)**
K_i	**Effective mass transfer coefficient for i component (1/s)**
Q^*_i	**Sorbent loading for i component in equilibrium (mol/kg)**
q_m	**Maximum sorbent loading (mol/kg)**
D_{AB}	**Diffusion coefficient (m^2/s)**
D_x	**Dispersion coefficient (m^2/s)**
L	**Bed height (m)**
L_w	**Bed wall thickness (m)**
m_{ads},	**Mass of adsorbent in the bed (g)**
F_i	**Molar flowrate of i component (mol/s)**
V_b	**Fixed-bed reactor volume (m^3)**

1. Introduction

Reduction of carbon dioxide (CO_2) emissions from power plants is essential to prevent global warming and climate change in future generations. The Intergovernmental Panel on Climate Change (IPCC) has indicated that climate scenarios will find it very difficult to achieve the 2°C target without CCS, since the cost of reaching the 2°C target will be 138% higher if carbon

capture is not included as a mitigation option [1,2]. It is a fact that nowadays coal is still one of the main energy resources for electricity production, together with natural gas [3].

Power plants fired by these fuels are one of the major sources of carbon dioxide emissions. In this scenario, further research on carbon capture and storage must be undertaken in order to apply the technology on a large scale. Lack of financial support from governments and expensive CCS technologies that are not practical in industry are major issues when implementing the technology [4–6].

On the one hand, carbon capture processes related to absorption are the most mature technology, and the first industrial carbon capture projects have been retrofitted in coal-fired power plants in Canada and the USA using solvent based absorption. This technology is easy to retrofit compared to other existing capture processes [7–9]. On the other hand, energy-intensive absorbent regeneration and solvent chemical properties that cause corrosion of the equipment and toxic products are the main disadvantages noted by most of the authors [10–13].

Adsorption processes applied to carbon capture have recently gained attention in research areas. High energy efficiency is one of the main advantages of the technology compared to processes using solvents, due to the ease of regeneration and not heating up large volumes of water during the recovery of the capture material [14].

Specifically, pre-combustion carbon capture applied to Integrated Gasification Combined Cycle (IGCC) power plants would use feed conditions with high pressures and ambient temperatures, which could considerably reduce the energy penalty of the capture process. Additionally, carbon dioxide concentrations in the fuel gas would be of around 30–50%, whereas in post-combustion the concentration of CO_2 is of around 10-15%. A binary gas mixture of hydrogen and carbon dioxide would enter the capture process in these plants,

59 coming from a water gas shift unit [15]. This would increase the degree of success of the
60 separation process.

61 The main pilot-scale projects developed in the field of pre-combustion carbon capture
62 applied to IGCC plants use physical absorption [16]. Pressure swing adsorption (PSA) applied
63 to these plants would improve the performance of the capture process since the process gas is
64 typically above 20 bar and PSA has been successfully implemented for hydrogen purification.
65 The key challenge for pre-combustion PSA is to develop a process step which efficiently
66 concentrates the carbon dioxide product [17].

67 For PSA to be successfully applied to IGCC power plants, both the material and engineering
68 factors must be considered [18]. In terms of the process materials, activated carbon (ACs)
69 adsorbents have been shown to be ideal candidates for the adsorption of carbon dioxide via
70 PSA, due to their structural stability, their relatively cheap price compared to that of other
71 adsorbents, and their high capacity and selectivity for carbon dioxide when the process operates
72 under PSA conditions (high pressures and ambient temperatures) [19–21]. The fact that
73 carbonaceous materials have high saturation capacities make them the most suitable adsorbents
74 for pre-combustion carbon capture using PSA [17].

75 Amine-modified activated carbons have been shown to be a promising material for carbon
76 dioxide capture, due to the chemical interaction between the nitrogen-enriched basic surface
77 and the acidity of CO_2. These materials show high selectivity for the adsorption of carbon
78 dioxide but further studies are required on the adsorption/desorption kinetics of these activated
79 carbons [17].

80 Most of the research carried out with amine-modified activated carbons focused on post-
81 combustion capture for temperatures between 30 and 60°C and ambient pressures of 1 bar [22–
82 24]. These adsorbents could potentially be more efficient in pre-combustion capture. One of

the main challenges of post-combustion capture would be to implement an adsorption capture system that can treat high flowrates of carbon dioxide at atmospheric pressures, temperatures of around 75°C, low carbon dioxide partial pressures, significant oxygen partial pressures and the presence of sulphur and nitrogen monoxides [7,15].

Some authors studied the adsorption behavior of chemical impregnated activated carbons for pre-combustion carbon dioxide capture. Zhu et al. [24] showed that the studied nitrogen enriched activated carbons demonstrated high uptake of CO_2 (9.3 wt%) at 0.15 bar and 25°C, due to their microporous surface and the nitrogen groups. However, previous studies did not show the effect that the synthesized activated carbons' surface and mass transfer properties could have on the breakthrough curves and on the overall purity of the products for pre-combustion binary gas mixtures.

Development of a PSA model that simulates the performance of the adsorbent in a fixed-bed reactor could help to identify the optimum adsorbent particle design and would enable to study the effect of the adsorbent properties on the gas product purity. In terms of PSA model validations, a study developed by Knox et al. [25] examined the accuracy of the parameter estimation with data from breakthrough curves when using both the mass transfer and dispersion coefficients as varying parameters, an approach used by several studies. The results of the study suggested that axial dispersion should be measured inside the bed as the experimental data can exhibit concentration front sharpening at the outlet of the bed. Then the mass transfer coefficient can be obtained via parameter estimation.

In this work, a PSA model has been compared to experimental breakthrough curves obtained from N_2 and CO_2 mixtures in a fixed-bed reactor, using TEPA-modified (AC-TEPA) and a novel MEA-MDEA-modified (AC-MEA-MDEA) activated carbon granules. The modified

106 activated carbons were compared with the unmodified activated carbons (AC-unmodified) in
107 a flow process, based on their capacity and the breakthrough time of the experiments.

108 The mass transfer coefficient of the modified adsorbents was determined using a Maximum
109 Likelihood Parameter Estimation algorithm developed by PSE (Process Systems Enterprise),
110 which minimizes the standard deviation between the model results and the experimental data
111 using an optimization problem. The response of the experimental adsorption process was
112 recorded at the outlet of the bed, when the adsorbing component (CO_2) appeared. The level of
113 dispersion of the fixed-bed reactor and the surrounding system was previously determined from
114 experimental data using glass beads inside the reactor.

115 This work also presents the results of a sensitivity analysis for a range of adsorbent properties
116 and process variables using PSA. This enables to identify the variables to which the purity of
117 the carbon dioxide and hydrogen gas products are more sensitive, such that the process can be
118 optimized.

119 Previous work studied the effect of the type of adsorbent [26] and the adsorbent properties
120 [27,28] on the performance of the carbon dioxide capture. Some authors also studied the effect
121 of the PSA process variables, such as the number of pressure equalization steps and the feed
122 pressure, on the capture performance [27,29]. This work adds a number of adsorbent
123 parameters and process variables (particle diameter and bed length to diameter ratio), as well
124 as, a carbon dioxide rinse step to previously reported PSA sensitivity analysis studies.

125

126 ## 2. Materials and methods

127 ### 2.1. Chemical impregnation procedure

128 Activated Carbon Norit® RB1 was selected as a precursor in this work, due to the
129 demonstrated high adsorption capacity and selectivity towards carbon dioxide.

130 Impregnation via solvents was selected to improve the overall adsorption performance of the
131 activated carbons. This process adds an amount of chemical solution to the surface of the
132 adsorbent, following the methodology proposed by Khalil [30].

133 The AC-MEA-MDEA was prepared by modifying the activated carbon surface with a blend
134 between Monoethanolamine (MEA) and Monodiethanolamine (MDEA) solvents, with a
135 concentration of 0.4 and 0.6 (molar basis), respectively. An amount of 20 g activated carbon
136 sample was placed in a beaker for impregnation. The MEA-MDEA solution (150 ml) was
137 prepared by the addition of 45 ml of each solvent in 60 ml of deionized water. This solution
138 was magnetically stirred at 500 rpm for thirty seconds, aiming the complete solvent dissolution.
139 Then, the amine solution was added to the beaker containing the activated carbon. The molar
140 ratio between the amines and the activated carbon was 1:0.6 (mol AC:mol MEA-MDEA).

141 The beaker was then stirred at 500 rpm for one hour at room temperature to enhance the
142 chemical interaction between the solvent and the activated carbon surface. The excess of
143 solvent was removed from the beaker with a pipette, and then the adsorbent was transferred to
144 a crucible boat and dried in an oven at 150^{o}C under nitrogen flow for 24 h.

145 The chemical treatment for the AC-TEPA (1:0.3, mol AC:mol TEPA) followed the same
146 order as the AC-MEA-MDEA. Instead, 150 ml of TEPA (90 ml of TEPA and 60 ml of
147 deionized water) solution was added to the activated carbons' surface. The activated carbons
148 were immersed in 150 ml of HCl 5M solution in a beaker and magnetically stirred at 500 rpm
149 for one hour. Deionized water was applied to remove the HCl excess in the activated carbons'
150 surface, and pH tapes were used to evaluate the neutralization of the material. Lastly, the
151 adsorbent was placed in the oven to dry for 24 hours at 150^{o}C.

2.2. Pressure Swing Adsorption (PSA) experimental studies with a fixed-bed reactor.

The dynamic adsorption behavior of the ACs was studied in a fixed-bed reactor (stainless steel; mass: 552.14 g; diameter: 2.5 cm; length: 6.9 cm; height: 2 cm), as shown in Figure 1. Mass flow controllers (Brooks 5850 thermal mass; nitrogen maximum flow rate: 400 $Nml.min^{-1}$; carbon dioxide maximum flow rate: 100 $Nml.min^{-1}$) (MFC, numbers 1 and 2) were used to keep a constant gas flowrate to the inlet of the bed, from carbon dioxide and nitrogen cylinders (both with purity of 99.99%) in the rig. Transducers (Swagelok S; pressure range: 0 – 42 bar) (numbers 3 and 12) worked as pressure sensors, which displayed the inlet and outlet pressure in a panel placed next to the rig.

Figure 1.

Numbers 4, 5 and 14 in Figure 1 show the bypass (Swagelok Stainless Steel Tee-Type Particulate Filter, 1/4 in), which works as a gas flow pathway to the reactor or directly to the exhaust (16). The adsorption temperature was monitored with two K-type thermocouples (7 and 9) placed in the inlet and outlet of the bed. A relief valve (Swagelok 316, pressure range: 24.1-51.7 bar) was used to secure safe operation and a back-pressure regulator (Swagelok 316 Stainless Steel PR Regulator, pressure range: 0 – 500 psig) (13) controlled the fixed-bed reactor pressure.

A CO_2 analyzer (SERVOFLEX MINIMP 5200) (10) measured the carbon dioxide concentration in the outlet of the reactor. Then the gas was directed to vent/exhaust (11). This equipment was calibrated for a low range (0%) with pure nitrogen (200 Nml/min) and a high range (100%) with pure carbon dioxide flow (100 Nml/min). The silica gel (dried at 140ºC overnight and then placed in the CO_2 analyzer inlet) was used as a drying agent, for the

175 accuracy of the CO_2 readings, as specified by the analyzer manufacturer. The placement of this
176 material did not interfere with the results reading.

177 The experimental adsorption tests with the ACs started by flowing pure nitrogen (200
178 Nml/min) into the bed (at 150ºC and 1 bar, for 3600 s), to remove residual gas components
179 from the system. The mass of the solid in the bed was 10 g for all experiments. When the bed
180 was completely pressurized to 25 bar, the nitrogen flow rate was reduced to 120 Nml/min and
181 the carbon dioxide flow started (80 Nml/min) to begin the adsorption test. The experiments
182 were conducted with 30% and 40% CO_2 feed fractions. The adsorption experiments lasted 1 h.
183 The amount of carbon dioxide adsorbed per mass unit of the activated carbons $\left(Q_{tCO_2}\right)$ was
184 determined from a mass balance (eq 1) applied to the bed during the adsorption experiments
185 and by integrating the area above the breakthrough curve.

186 $$Q_{tCO_2} = \frac{1}{m_{ads}} \left[\int_0^t \left(F_{CO_2,in-} F_{CO_2,out}\right) dt - \frac{Y_{CO_2,feed} P V_b}{RT}\right] \quad (1)$$

187 where, $m_{adsorbent}$ corresponds to the mass of adsorbent in the fixed-bed reactor, $F_{CO_2,in}$ and
188 $F_{CO_2,out}$ are the molar flowrates of carbon dioxide at the inlet and outlet of the bed, respectively.
189 t_s is the time to achieve the saturation of the adsorbent, $Y_{CO_2,feed}$ is the molar fraction of carbon
190 dioxide in the feed stream. P and T are the pressure and temperature of the bed, V_b is the bed
191 volume and R is the universal gas constant.

192

193 **3. Theory**

194 The adsorption step of PSA was compared to a one-dimensional model that included 30%
195 CO_2 and 70% N_2, as well as, 40% CO_2 and 60% N_2 mol percentages in the feed at 25 bar and
196 ambient temperatures (25ºC), the same as the laboratory conditions.

The main assumptions underlying the partial algebraic differential equations (PADEs) used in the PSA model were the following, supported by previous studies [15, 30–36]:

• The Soave-Redlich-Kwong equation of state was used to calculate the compressibility factor for this system, where the value was over 0.9. Therefore, flowing gases were considered ideal.

• There were no radial variations in pressure, temperature, and concentration of the components in the gas and solid phases.

• The solid and gas phases were in thermal equilibrium and the bulk density of the solid remains constant.

These assumptions were incorporated when developing the PADEs that define the evolution of the concentration of the components (overall and component mass balances) and temperature (energy balance) in the fixed-bed reactor.

The overall (eq 2) and component (eq 3) mass balance equations were developed including the accumulation, inlet and outlet, adsorption and dispersion terms of the reactor. The energy balance (eq 4) equation assumed the heat accumulation in the solid and the gas phase, heat transfer in the gas phase, the heat generated from adsorption and heat transfer from the gas phase to the reactor wall.

$$\varepsilon_t \frac{\partial C(z)}{\partial t} = -\varepsilon_b \frac{\partial (C(z)v(z))}{\partial z} + \varepsilon_b D_x \frac{\partial^2 C(z)}{\partial z^2} - (1-\varepsilon_b) \sum_{i=1}^{N_{comp}} \frac{\partial Q(i,z)}{\partial t}) \quad (2)$$

$$\varepsilon_t \frac{\partial Y(i,z)}{\partial t} = -\varepsilon_b v(z) \frac{\partial Y(i,z)}{\partial z} + \varepsilon_b D_x (\frac{\partial^2 Y(i,z)}{\partial z^2} + \frac{2}{C(z)} \frac{\partial Y(i,z)}{\partial z} \frac{\partial C(z)}{\partial z}) - \frac{(1-\varepsilon_b)}{C(z)} (\frac{\partial Q(i,z)}{\partial t} - Y_{(i,z)} \sum_{i=1}^{N_{comp}} \frac{\partial Q(i,z)}{\partial t}) \quad (3)$$

$$ec_{p,g(z)}\frac{\partial(T(z)v)}{\partial z}+\varepsilon_t ec_{p,g(z)}\frac{\partial T(z)}{\partial t}+\varepsilon_t e_s c_{p,s}\frac{\partial T(z)}{\partial t}-(1-\varepsilon_b)e_s\sum_{i=1}^{N_{comp}}\Delta H_{ads(i)}\frac{\partial Q(_i,z)}{\partial t}+$$

$$h_i(T(z)-T_{wall)}=\lambda\frac{\partial^2 T(z)}{\partial z^2} \quad (4)$$

The dispersion coefficient was determined comparing a dispersion model with the glass-beads experiments, using parameter estimation. The fixed-bed reactor was filled with glass beads of the same size of the activated carbons. The dispersion model included the inlet pipe (ID= 1×10^{-3} m, L= 0.5 m), which connected the CO_2 and N_2 feed vessels with the fixed-bed reactor and the outlet pipe (ID= 1×10^{-3} m, L= 0.1 m), which connected the reactor with the CO_2 analyzer. This system was isothermal as adsorption did not occur in the beads and the reactor wall was isolated. Eq 5 shows the mass balance equation for the dispersion model for the reactor filled with glass beads and the surrounding system.

$$\frac{\partial Y(z)}{\partial t}=-v\frac{\partial(Y(i,z))}{\partial z}+D_x\frac{\partial^2 Y(i,z)}{\partial z^2} \quad (5)$$

The equilibrium between the gas phase and the activated carbons' surface was represented by the Langmuir isotherm (eq 6), based on the equilibrium data obtained for the activated carbons from the HPVA experiments (Appendix A, Figures A1 and A2). The Ergun equation (eq 7) was used to calculate momentum losses [15,31,34,35].

The limiting step of mass transfer resistance is diffusion through micro-pores, represented by the linear driving force (LDF) model (eq 8), which describes the adsorption kinetics [15,31–33,36]. This assumption is supported by a previous study, where this simplification was shown to be valid for PSA systems featuring activated carbons [35].

$$Q^*_{(z)}=\frac{q_m bP(z)RT(z)}{1+bP(z)RT(z)} \quad (6)$$

$$\frac{\partial P(z)}{\partial Z}=150\,u_{g(z)}\frac{(1-\varepsilon_b)^2}{D_p^2\varepsilon_t^3}+1.75\frac{(1-\varepsilon_t)}{D_p\varepsilon_t^3}\,e\,v(z)/v(z)/ \quad (7)$$

$$\frac{\partial Q_{(i,z)}}{\partial t} = K_{(i)}(Q^*_{(i,z)} - Q_{(i,z)}) \quad (8)$$

The results of the model were obtained using gPROMS® ProcessBuilder 1.1.0. The custom model was developed in the gPROMS® language environment, where the model was divided into various subtasks: specification of parameters, variables, boundary conditions, and equations.

The thermodynamics of the process were calculated using the Multiflash® package. The backward finite difference method (BFDM) was used to discretize the component and overall concentrations, velocity, and temperature variables (against the flow, due to the diffusion phenomena). However, the pressure was discretized using the forward finite difference method (FFDM), as the pressure was specified in the outlet of the bed.

The boundary conditions of the model are shown in eqs 9–18. The inlet boundary conditions for the fraction of the components and temperature variables changed for each step of the PSA model, by introducing discontinuities that cause sudden changes in these variables. The outlet boundary condition of the pressure (P_{end}) was kept constant for the adsorption (25 bar), purge and rinse (1 bar) steps.

$$-\varepsilon_b D_x \frac{\partial C_i}{\partial z}_{z=0} = v_{z=0}(C_{i,feed} - C_{i,z=0}) \quad (9)$$

$$-\varepsilon_b \lambda \frac{\partial T}{\partial z}_{z=0} = v_{z=0} e c_{p,g,z=0}(T_{feed} - T_{z=0}) \quad (10)$$

$$v_{z=0} = v_{feed} \quad (11)$$

$$\frac{\partial C_i}{\partial z}_{z=L} = 0 \quad (12)$$

$$\frac{\partial T}{\partial z}_{z=L} = 0 \quad (13)$$

$$\frac{\partial v}{\partial z}_{z=L} = 0 \quad (14)$$

$$P_{z=L} = P_{end} \quad (15)$$

For the pressurization (press), pressure depressurization (depress), and pressure equalization (equal) steps, the outlet boundary condition of the pressure was described by a transition equation (eq 16–18), between the adsorption pressure (P_{ads}), equalization pressure (P_{eq}) and the atmospheric pressure (P_{atm}). The change was described by a linear equation that modelled a linear valve.

$$\frac{\partial P_{press}}{\partial t}_{z=L} = \left(\frac{P_{ads} - P_{atm}}{t_{pressurization}}\right) \quad (16)$$

$$\frac{\partial P_{depress}}{\partial t}_{z=L} = \left(-\frac{P_{eq} - P_{atm}}{t_{depressurization}}\right) \quad (17)$$

$$\frac{\partial P_{equal}}{\partial t}_{z=L} = \left(-\frac{P_{ads} - P_{eq}}{t_{equalization}}\right) \quad (18)$$

The parameters used in the model (adsorbent and bed properties) are shown in Table 1. The conditions are the same as those for the laboratory experiments. The Langmuir isotherm parameters and the heat of adsorption were determined from the HPVA data of the activated carbons. The axial heat dispersion coefficient and the effective heat transfer coefficient were calculated using the Wakao and Funazkri correlations [37–39]. Initially (at t = 0), it is assumed that there is only nitrogen at high pressures (25 bar) and ambient temperatures (25°C) in the fixed-bed, and no carbon dioxide on the surface of the adsorbent.

Table 1. Adsorbent and fixed-bed reactor parameters for the Pressure Swing Adsorption model.

Amine-modified ACs data		Fixed-bed reactor data	
Particle density, e_s (kg m^{-3})	262	Bed length, L (m)	0.069
Particle void fraction, ε_p	0.74	Bed void fraction, ε_b	0.48
Particle diameter, d_p (m)	0.001	Bed length/diameter ratio, L/D	2.76
Sorbent specific heat, cp_s (kJ kg^{-1} K^{-1})	1	Wall specific heat, cp_w (kJ kg^{-1} K^{-1})	0.46
Adsorption heat CO_2, ΔH (kJ mol^{-1})	24.8	Wall thickness, L_w (m)	0.002
Adsorption heat N_2, ΔH (kJ mol^{-1})	8.4	Wall density, e_w (kg m^{-3})	7700
Maximum monolayer coverage capacity for CO_2, $q_{m,CO2}$ (mol kg^{-1})	9.2	Effective heat transfer coefficient, h_i (kW m^{-2} K^{-1})	500
Langmuir equilibrium constant for CO_2, b_{CO2} (Pa^{-1})	$3x10^{-6}$	Axial heat dispersion coefficient, λ (W m^{-1} K^{-1})	1.5

4. Results and discussion

4.1. Performance of the novel MEA-MDEA-modified ACs under PSA conditions.

The experimental breakthrough data from the adsorption step was generated using a binary mixture of CO_2 and N_2 (40% and 60%, molar basis) at 25ºC and 25 bar, using the AC-Unmodified and the AC-MEA-MDEA in the fixed-bed reactor, one at a time.

Nitrogen was used instead of hydrogen to test the adsorption behavior of the adsorbents in pre-combustion conditions, due to safety concerns and to the fact that the performance of the CO_2-H_2 mixture was expected to be far more efficient than that of CO_2-N_2 mixture. This is due to the light weight of the hydrogen gas compared to nitrogen. A study by Garcia et al. [40] on AP3-60 activated carbons showed that the fraction of carbon dioxide captured for a CO_2- N_2

291 mixture was ~0.82 of the total volume of gas captured, whereas it was ~0.92 for a CO_2-H_2
292 mixture.

293 The comparison between the two systems was quantified using previous studies, which
294 measured the adsorption capacity of the activated carbons for CO_2-N_2 and CO_2-H_2 systems. In
295 the studies that compared adsorbent capacities, the capacity of the activated carbons to adsorb
296 hydrogen varied between 0.04 and 0.06 mmol/g [35,38,41], whereas the capacity of the
297 activated carbons to absorb carbon dioxide varied between 9 to 10 mmol/g. The adsorbed
298 carbon dioxide in the breakthrough experiments for this study was 9.6 mmol/g for the
299 unmodified activated carbon, whereas it was 10.6 mmol/g for the AC-MEA-MDEA. The
300 adsorbent capacity of nitrogen reported by Lopes et al. [39] was 0.14 mmol/g, which was
301 similar to the capacity of the activated carbons to adsorb hydrogen.

302 Figure 2 shows the breakthrough curves obtained for the experiments with the AC-MEA-
303 MDEA and the AC-Unmodified adsorbents at 25 bar. The total amount of carbon dioxide
304 adsorbed per mass unit of the adsorbent was calculated by integrating the area above the
305 breakthrough curve, following eq 1. The AC-MEA-MDEA adsorbed 10.6 mmol CO_2/g
306 adsorbent, whereas the AC-Unmodified adsorbed 9.6 mmol CO_2/g adsorbent.

307 **Figure 2.**

308 The amine modified activated carbons showed good results for post-combustion capture
309 conditions using 15% CO_2 and 85% H_2 feed conditions in previous studies [22]. These
310 adsorbents show far promising results for pre-combustion capture using 40% CO_2 and 60% N_2
311 mixtures, as shown in Figure 2.

312 Additionally, the AC-MEA-MDEA showed improved selectivity for carbon dioxide
313 compared to the AC-Unmodified. This was analyzed by measuring the amount of nitrogen

leaving the fixed-bed reactor during the experiments (Appendix B, Table B1). The amount of nitrogen that left the bed during the adsorption experiment was 7625 mg with the AC-Unmodified, whereas this amount was 8733.1 mg in the experiment using AC-MEA-MDEA. From these values it was derived that the amount of pure nitrogen produced with the AC-MEA-MDEA was 15% higher.

The later break-point (1274 s) for the experiment using AC-MEA-MDEA, compared to the experiment with the AC-Unmodified (992 s), is mainly due to the improved capacity of the amine-modified adsorbent compared to the precursor. The steeper breakthrough curve of the AC-MEA-MDEA also shows an improved mass transfer between the gas and the solid surface. This can be explained by the incorporation of the active amine sites in the porous surface of the carbons [42–44] and supports the success of the novel surface modification.

4.2. Model validation via parameter estimation and ACs mass transfer coefficient determination.

In order to ensure the accuracy of the parameter estimation between the model and the activated carbons, the dispersion coefficient was firstly obtained by fitting a dispersed plug flow model (eq 5) against experimental data using glass beads under CO_2-N_2 mixtures and PSA experimental conditions.

Figure 3 shows the breakthrough curves for the plug-flow model and the experimental data for the glass beads only, which enabled to predict the dispersion coefficient to be $5 \times 10^{-6} m^2 s^{-1}$. The dispersion coefficient was then fixed at the value derived from the glass beads to enhance the accuracy of the parameter estimation between the PSA model and the laboratory experiments with the amine modified ACs [25]. The mass transfer coefficient was the parameter estimated from this fit.

Figure 3.

Once the dispersion coefficient was determined, the mass transfer coefficients of, both, AC-MEA-MDEA and AC-TEPA activated carbons were compared. Figure 4a and Figure 4b show the breakthrough curves for the parameter estimation for each of the surface modified ACs, using 40% and 30% CO_2 fractions in the feed gas.

Figure 4a.

Figure 4b.

A good visual fit was achieved between the experiments and the model for both of the adsorbents, with a sum of squared residuals (SSR) of 0.1% (a) and 0.3% (b), which is under the 10% of the acceptable percentage for engineering purposes using parameter estimation. The PSA model predicted accurately the breakthrough curves for the experiments using 30% and 40% CO_2 feed fraction with AC-MEA-MDEA and, 30% feed fraction with the AC-TEPA. The PSA model using 40% CO_2 feed fraction with AC-TEPA showed a steeper breakthrough curve than the one showed by the experiment, due to the chemisorption effects that may have been introduced with the amine groups in the activated carbon surface. The results for the mass transfer coefficient of the AC-MEA-MDEA and the AC-TEPA were $0.046\ s^{-1}$ and $0.074\ s^{-1}$, respectively, and they are in the range of previously reported values for PSA processes using activated carbons [15].

Although the AC-TEPA showed a greater mass transfer value and, thus, a steeper breakthrough curve, the AC-MEA-MDEA showed to have a later break-point with around 3 to 4 minutes difference for both CO_2 feed fractions, due to their high capacity as shown in the previous chapter. This could be explained by the insertion of a two-amine group solution (MEA and MDEA) into the pores, instead of the insertion of a one-amine group solution, as reported in previous publications [17].

362

363 **4.3. Effect of the adsorbent properties on the overall purity of H_2 and CO_2**

364 After the model verification, a seven-step PSA model was developed which considered a
365 mixture of 40% carbon dioxide and 60% hydrogen entering the fixed-bed reactor. This process
366 simulated the conditions of a pre-combustion PSA process in an IGCC power plant. Table 2
367 shows the steps adopted in the model, which used Eqs 2-8 and Eqs 9-18 (boundary conditions)
368 to obtain the simulation results. Figure 5 shows the cycle sequence used in the PSA simulations.

369 **Table 2.** Conditions for the seven-step PSA model.

Steps	Description
Pressurization (P)	The fixed-bed is pressurized to 25 bar with a mixture of H_2 and CO_2
Adsorption (A)	Adsorption of CO_2 in the surface of the adsorbent at 25 bar. Hydrogen is obtained as a product
Pressure equalization-depressurization (PE-D)	The bed pressure is decreased to 12.5 bar (the midpoint between the adsorption and the purge pressure) when connecting to a pressurizing bed
Depressurization (D)	The bed pressure is further decreased to 1 bar. The product gas goes to a purging bed.
Rinse (R)	CO_2 enters the bed at 1 bar. CO_2 is obtained as a product
Purge (Pu)	H_2 enters the bed at 1 bar, coming from the depressurization step. CO_2 is obtained as a product
Pressure equalization-pressurization (PE-P)	The bed pressure is increased to 12.5 bar (the midpoint between the purge and the adsorption pressure) when connecting to a depressurizing bed

370

371 **Figure 5.**

The process conditions used in the simulation were the same as those in the laboratory experiments at ambient temperatures and feed pressures for the pressurization and adsorption step, namely of 25 bar, and for the purge and the rinse step, namely 1 bar. Eq 19-20 were used to study the effect of the adsorbent properties on the overall purity of the carbon dioxide (Pu_{CO_2}) and hydrogen (Pu_{H_2}) products. The adsorbent parameters were independently varied.

$$Pu_{CO_2} = \frac{\int_{t=t_{rinse}}^{t=t_{purge}} C_{CO_2,z=L} v_{z=L} dt}{\sum_{i=1}^{n} \int_{t=t_{rinse}}^{t=t_{purge}} C_{i_{z=L}} v_{z=L} dt} \quad (19)$$

$$Pu_{H_2} = \frac{\int_{t=0}^{t=t_{feed}} C_{H_2,z=L} v_{z=L} dt}{\sum_{i=1}^{n} \int_{t=0}^{t=t_{feed}} C_{i_{z=L}} v_{z=L} dt} \quad (20)$$

Firstly, the results of the mass transfer coefficient sensitivity analysis are illustrated in Figure 6, which shows the evolution of the molar fraction of carbon dioxide at the end of the fixed-bed reactor for the seven-step pressure swing adsorption model. The break-point of the feed step does seem to be affected by variations in the mass transfer coefficient. With an increase from 0.02 s^{-1} to 0.1 s^{-1} in the mass transfer coefficient, the break-point occurs around two minutes later. The slope between the adsorption and, the purge and rinse steps remains constant, due to the depressurization of the bed before the break-point caused by the adsorbents' saturation. This step decreases the pressure in the bed and creates a pressure gradient between the inlet and the outlet of the bed. Carbon dioxide is not desorbed until the end of the bed reaches pressures of around 1 bar.

Secondly, the results for the rest of the adsorbent property values used in the sensitivity analysis are shown in Table 3, together with the carbon dioxide and hydrogen purity values obtained for each parameter value. The laboratory (default) values for those properties are shown with an asterisk in the table.

For the particle diameter (PD), the sensitivity analysis was simulated with a deviation of 25% from the original size. Smaller particles may cause pressure drop issues. For the particle and bed void fraction and for the mass transfer coefficient, the values were selected based on the previous numbers shown for activated carbon adsorbents [23,24,44].

Figure 6.

Table 3 shows that the mass transfer coefficient is the variable that had the greatest effect on the overall purities of CO_2. The purities of hydrogen did not deviate from 99% when changing this variable. The values of the breakthrough capacity for carbon dioxide remain constant when varying the mass transfer coefficient. The same was observed for the rest of the adsorbent properties.

The most common correlation that has been used to calculate the mass transfer coefficient is that shown by Farooq and Ruthven, which sums the micro-, meso- and macro-pore mass transfer resistances [45]. This variable can also be calculated using the Peclet number correlation [46] . These correlations have shown to be uncertain due to dispersion effects in the bed [25]. In this study the mass transfer coefficient has been varied independently and the results show that an adsorbent which shows a high mass transfer coefficient towards carbon dioxide (of around 0.1 s^{-1}) enables to obtain a higher purity, of around 10%, in the final CO_2 product, compared to lower mass transfer coefficient values of around 0.04 s^{-1}. The mass transfer coefficient affects the break-point (Figure 6) and, thus, the amount of carbon dioxide adsorbed and the purity of the CO_2 product stream in the rinse and purge steps (between 1100 and 1700s).

Table 3. Calculated Purity (%) Values for the H_2 and CO_2 Products Streams for a Number of Adsorbent Properties.

Particle diameter (m)	Purity H_2/CO_2 (%)	Particle void fraction (-)	Purity H_2/CO_2 (%)
0.75×10^{-3}	99.5/82.1	0.55	99.4/82.7
1×10^{-3}*	99.4/81.9	0.74*	99.4/81.9
1.25×10^{-3}	99.3/81.6	0.85	99.4/81.6
Bed void fraction (-)	**Purity H_2/CO_2 (%)**	**MT coefficient (s^{-1})**	**Purity H_2/CO_2 (%)**
0.48*	99.4/81.9	0.02	99.2/71.9
0.6	99.4/81	0.04*	99.4/81.9
0.7	99.5/80.8	0.1	99.5/90.3

In terms of the particle and bed void fractions and the particle diameter, the purity of hydrogen does not seem to be affected by those properties and remains constant at 99%, with a marginal error of $\pm$ 0.1%. A plausible explanation for this is that if the adsorbent properties are in an acceptable range for the adsorption of carbon dioxide, the outcome of hydrogen product stream will be highly pure (over 99%), due to the lightness of the hydrogen gas and the high affinity of the carbonaceous surface with the carbon dioxide gas for binary mixtures.

The purity of carbon dioxide gas is more sensitive to the properties of the adsorbent applied in the given process conditions and is about 20%–30% lower than the purity of hydrogen, as reported in most industrial processes where the light product (hydrogen) is the desired product [35]. Decreasing the particle diameter favorably increases the purity of the CO_2 stream, due to the greater external surface areas for adsorption in the fixed-bed reactor. It also favors the plug flow in the bed, because the ratio of the bed to the particle diameter increases [25].

The recovery of the hydrogen and carbon dioxide products remained practically constant varying the adsorbent properties. The recovery of carbon dioxide was around 52% for this process, whereas it was around 75% for the hydrogen product. The recovery of these products decreased, due to recycling hydrogen and carbon dioxide into the process, compared to previous studies [27,29].

435 **4.4. Effect of the PSA process variables on the overall purity of H_2 and CO_2**

436 The sensitivity analysis for the seven-step PSA process variables (component feed fractions,
437 feed and purge pressures and reactor length to diameter ratio) was carried out the same way as
438 for the adsorbent properties, using eqs 2-20. The adsorbent properties in the model were set to
439 be the same as the AC-MEA-MDEA properties (Table 1) with a mass transfer coefficient value
440 of $0.046\ s^{-1}$.

441 The results for the process variables (feed pressure and feed component fractions) that had
442 the greatest effect on the breakthrough curves are illustrated in Figures 7-8. For the purpose of
443 consistency, one process variable value at a time was changed from the original laboratory
444 process. The process variable values used in the sensitivity analysis are shown in Table 4,
445 together with the carbon dioxide and hydrogen purity values obtained from the variable values.

446 The laboratory (default) values for those variables are shown with an asterisk in Table 4. The
447 rest of the values of Table 4 where selected based on previous conditions given in PSA process
448 studies [31–33,39]. The molar feed fraction of carbon dioxide was varied from 0.3 to 0.6 in
449 order to study the effect of the feed concentration of CO_2 in the adsorption step, with a view to
450 future work, to consider a carbon dioxide product recycle stream featuring a compressor.

451 Input purge pressures were decreased lower than atmospheric pressures (Table 4) in order to
452 investigate the need of a vacuum swing adsorption process. The reactor's length to diameter
453 ratios did not deviate more than 50% of the original value, due to design standards of process
454 engineering.

455 **Figure 7.**

456 **Figure 8.**

Figures 7 and 8 show that the selected process variables have a greater effect than the adsorbent properties on the overall CO_2 purities. On the one hand, the values of the breakthrough capacity remain constant, as do those of the adsorbent properties. On the other hand, the break-point of the feed step is greatly affected by variations in these variables.

Table 4. Calculated Purity (%) Values for the H_2 and CO_2 Products Stream for a Number of PSA Process Variables.

Feed pressure (Pa)	**Purity H_2/CO_2 (%)**	**Purity H_2/CO_2 (%)**	**Purity H_2/CO_2 (%)**
15×10^5	99.4/74.8	0.5×10^5	99.4/96.4
20×10^5	99.4/79.2	1×10^5*	99.4/81.9
25×10^5*	99.4/81.9	1.5×10^5	99.4/77
CO_2 feed fraction (-)	**Purity H_2/CO_2 (%)**	**Reactor length/ diameter ratio (-)**	**Purity H_2/CO_2 (%)**
0.3	99.3/73	2.5	99.5/84.7
0.4*	99.4/81.9	2.76*	99.4/81.9
0.6	99.5/91.6	3.5	99.1/79.5

The feed pressure (P_{feed}) affects only the overall purity of the carbon dioxide at high pressures (>15 bar). This can be due to the increase of the pressure ratio between the adsorption and purge step, which increases the CO_2 partial pressure in the pressure equalization and depressurization step. Although the purity of hydrogen is not affected, an increase of 5 bar in the feed pressure delays the break-point by 2 minutes (Figure 7). This explains why the overall purity of carbon dioxide is higher in the purge step. The total uptake of CO_2 increases due to a longer adsorption time, considering all PSA processes have the same duration.

The purge pressure has a greater effect than the feed pressure on the total purity of carbon dioxide as shown in Table 4. This is because the larger trade-off between the adsorption and the purge pressure when the last variable decreases to vacuum values and CO_2 is obtained as a product in the purge and rinse steps. The increase in the pressure gradient causes higher

476 depressurization rates, which enables a purer CO_2 stream of about 96.4% at vacuum pressures
477 of 0.5 bar. At this stage, a cost analysis should be estimated, to see whether it is worth including
478 a vacuum generator in the process.

479 The feed fraction of carbon dioxide in the adsorption step (Y_{feed}) has a greater effect on the
480 break-point than do both the purge and the feed pressures, as shown in Figure 8. With an
481 increase of about 20% in the feed fraction, the purity of carbon dioxide increases around 10%.
482 This enhances the mass transfer between the gas and the carbonaceous surface. At this stage,
483 it may be useful to introduce a recycle stream from the depressurization to the adsorption step,
484 which would increase the carbon dioxide partial pressure in the inlet of the reactor, supported
485 by most of the studies [31–33]. This would require a compressor in the recycle stream.

486 In terms of the reactor design, smaller length to diameter ratios yielded a higher purity of
487 carbon dioxide product (Table 4). When the ratio is about 10% smaller than that of the standard
488 laboratory reactor, the purity of carbon dioxide is 3% higher. A plausible explanation for this
489 could be the decreasing carbon dioxide partial pressure as the feed gas goes through the reactor,
490 which decreases the mass transfer driving force between the gas and the solid surface. Greater
491 diameters would enable higher adsorbent densities in the inlet of the bed, increasing the
492 adsorption capacity of the fixed-bed reactor in the inlet, where the carbon dioxide concentration
493 is at feed concentrations.

494 Deviant values on PSA process variables had a greater effect on the final purity of carbon
495 dioxide than did values of the adsorbent properties. The results showed that the process could
496 be scaled up using the parameters for amine-modified activated carbons and by including a
497 measure for the uncertainty of the adsorbent properties. These properties could cause a
498 maximum deviation of $\pm 10\%$ in the CO_2 product purity.

499 The PSA process variables, specifically, the feed fractions, the purge and feed pressures
500 seem to have a greater effect on the final CO_2 purity, with deviations of $\pm$ 10 to 20% in the
501 final purity values. Carbon dioxide concentrations of around 60% at 25 bar are preferred in the
502 feed during the adsorption step and 0.5 bar pressures in the purge and rinse steps.

503 The overall recovery of the hydrogen and carbon dioxide products was less sensitive
504 compared to the purity of these products, by varying these process conditions. The recovery
505 values obtained with the standard case (conditions shown with an asterisk in Table 4), were
506 52% and 75% for carbon dioxide and the hydrogen, respectively. These recovery values
507 deviated no more than 2% by varying the process conditions, because the amount of the
508 component products used in each step was not varied.

509 This sensitivity analysis shows that over 90% pure carbon dioxide cannot be obtained in the
510 basic case, but by varying the PSA process conditions, such as introducing a vacuum generator
511 to reach purge pressures of 0.5 bar or recycling carbon dioxide into the feed, purities of about
512 95% would be achieved. These results could be relevant and tested further at a larger scale. In
513 this case, the inclusion of a compressor or a vacuum generator would lead to a significant
514 increase of the energy penalty and the advantages in terms of separation performance would
515 thus need to be weighed against the disadvantage in terms of the energy efficiency of the
516 process.

517

518 ## 5. Conclusions

519 A laboratory scale adsorption step under pre-combustion PSA conditions for IGCC power
520 plants was compared to a PSA model, using AC-TEPA and the novel AC-MEA-MDEA
521 modified activated carbons. The AC-MEA-MDEA adsorbents showed promising results

compared to the unmodified commercial Activated Carbon Norit®, in terms of the carbon dioxide adsorbed (of around 10% higher) and selectivity during the adsorption experiments in a fixed-bed reactor.

A parameter estimation between an experimental adsorption step using AC-TEPA and AC-MEA-MDEA adsorbents and a PSA model, showed a good fit between the breakthrough curves, with an SSR less than 10%. Although the AC-TEPA showed a greater mass transfer coefficient ($0.074\ s^{-1}$), the delayed break-point (of around 200 s) of the AC-MEA-MDEA adsorbents, makes them more promising for pre-combustion PSA.

A sensitivity analysis of the effect of the adsorbent properties showed that these variables had a greater effect on the purity of carbon dioxide than on the purity of the hydrogen in the product stream. The properties of the amine-modified adsorbents are important for obtaining highly purified products (99.4% for hydrogen and 81.9% for carbon dioxide), specifically for the purity of the light product stream.

A sensitivity analysis of the process variables of PSA showed that modifications in these variables could yield to higher purities of CO_2 product stream (over 90%). Sensitivity analyses showed that purities of carbon dioxide and hydrogen, as high as 91.6% and 96.4%, respectively, could be achieved by increasing the carbon dioxide feed fraction by 50% and decreasing the purge pressure by 50%. For these cases, the additional capital and operational costs should be investigated, as there would be a need for a compressor for the recycle stream and a vacuum generator to obtain pressures under atmospheric conditions. The recovery of these products did not seem greatly affected by variations of the adsorbent properties and process variables, with a maximum of 2% deviation varying the PSA process variables.

545 **Acknowledgements**

546 This work was supported financially by the Brazilian National Council for Scientific and
547 Technological Development (CNPq) from the program Science Without Borders (SwB,
548 206095/2014-7), as well as, the EPSRC and the Centre for Doctoral Training of Carbon
549 Capture and Storage and Cleaner Fossil Energy (EP/L016362/1). gPROMS® ProcessBuilder
550 software was provided in-kind by Process Systems Enterprise. Experimental data are available
551 at epapers.bham.ac.uk

552

553 **Supplementary data file: Appendix A and B**

554 Supplementary data of this article can be found online.

References

[1] Global CCS Institute. Paris climate change targets cannot be met without CCS: COP23. vol. 30. Bonn, Germany.: 2017.

[2] Edenhofer O, Pichs-Madruga R, Sokona Y, Farahani E, Kadner S, Seyboth K, et al. Mitigation of Climate Change. 2014. doi:10.1017/CBO9781107415416.

[3] U.S. Energy Information Administration (EIA). International Energy Outlook 2016. vol. 0484(2016). Washington, DC: Office of Energy Analysis; 2016.

[4] DOE/NETL. Advanced Carbon Dioxide Capture R&D Program: Technology Update. Pittsburgh, PA: 2013.

[5] Wheeler D, Ummel K. Calculating CARMA: Global Estimation of CO_2 Emissions from the Power Sector. 2008.

[6] Ummel K. Carma Revisited: An Updated Database of Carbon Dioxide Emissions from Power Plants Worldwide. SSRN Electron J 2012:2226505. doi:10.2139/ssrn.2226505.

[7] Aaron D, Tsouris C. Separation of CO_2 from flue gas: A review. Sep Sci Technol 2005;40:321–48. doi:10.1081/SS-200042244.

[8] Kohl AL, Nielsen RB. Gas Purification. vol. 10. 5th ed. Houston, TX. USA: Gulf Professional Publishing; 1997. doi:10.1016/B978-088415220-0/50009-4.

[9] Campbell JM. Gas conditioning and processing. 4th ed. Norman, Okla.: Campbell Petroleum Series; 1998.

[10] Cormos CC. Evaluation of reactive absorption and adsorption systems for post-combustion CO_2 capture applied to iron and steel industry. Appl Therm Eng 2016;105:56–64. doi:10.1016/j.applthermaleng.2016.05.149.

[11] Ebner AD, Ritter JA. State-of-the-art adsorption and membrane separation processes for carbon dioxide production from carbon dioxide emitting industries. vol. 44. 2009. doi:10.1080/01496390902733314.

[12] Gray ML, Soong Y, Champagne KJ, Pennline H, Baltrus JP, Stevens RW, et al. Improved immobilized carbon dioxide capture sorbents. Fuel Process Technol 2005;86:1449–55. doi:10.1016/j.fuproc.2005.01.005.

[13] Houshmand A, Shafeeyan MS, Arami-Niya A, Daud WMAW. Anchoring a halogenated amine on the surface of a microporous activated carbon for carbon dioxide capture. J Taiwan Inst Chem Eng 2013;44:774–9. doi:10.1016/j.jtice.2013.01.014.

[14] Liu H, Liu B, Lin LC, Chen G, Wu Y, Wang J, et al. A hybrid absorption-adsorption method to efficiently capture carbon. Nat Commun 2014;5:1–7. doi:10.1038/ncomms6147.

[15] Agarwal A, Biegler LT, Zitney SE. Superstructure-Based Optimal Synthesis of Pressure Swing Adsorption Cycles for Precombustion CO_2 Capture. Ind Eng Chem Res 2010;49:5066–79. doi:10.1021/ie900873j.

[16] Jansen D, Gazzani M, Manzolini G, Dijk E Van, Carbo M. Pre-combustion CO_2 capture. Int J Greenh Gas Control 2015;40:167–87. doi:10.1016/j.ijggc.2015.05.028.

[17] Abanades JC, Wiley DE, Mangano E, Li H, Ho MT, Mattisson T, et al. Emerging CO_2 capture systems. Int J Greenh Gas Control 2015;40:126–66. doi:10.1016/j.ijggc.2015.04.018.

[18] Grande CA. Advances in Pressure Swing Adsorption for Gas Separation. ISRN Chem Eng 2012;2012:1–13. doi:10.5402/2012/982934.

[19] Hao G-P, Li W-C, Lu A-H. Novel porous solids for carbon dioxide capture. J Mater

Chem 2011;21:6447. doi:10.1039/c0jm03564e.

[20] Di Biase E, Sarkisov L. Molecular simulation of multi-component adsorption processes related to carbon capture in a high surface area, disordered activated carbon. Carbon N Y 2015;94:27–40. doi:10.1016/j.carbon.2015.06.056.

[21] Jordá-Beneyto M, Suárez-García F, Lozano-Castelló D, Cazorla-Amorós D, Linares-Solano A. Hydrogen storage on chemically activated carbons and carbon nanomaterials at high pressures. Carbon N Y 2007;45:293–303. doi:10.1016/j.carbon.2006.09.022.

[22] Samanta A, Zhao A, Shimizu GKH, Sarkar P, Gupta R. Post-Combustion CO_2 Capture Using Solid Sorbents: A Review. Ind Eng Chem Res 2012;51:1438–63. doi:10.1021/ie200686q.

[23] Shafeeyan MS, Houshmand A, Arami-Niya A, Razaghizadeh H, Daud WMAW. Modification of Activated Carbon Using Nitration Followed by Reduction for Carbon Dioxide Capture. Bull Korean Chem Soc 2015;36:533–8. doi:10.1002/bkcs.10100.

[24] Zhu B, Li K, Liu J, Liu H, Sun C, Snape CE, et al. Nitrogen-enriched and hierarchically porous carbon macro-spheres-ideal for large-scale CO_2 capture. J Mater Chem A 2014;2:5481–9. doi:10.1039/c4ta00438h.

[25] Knox JC, Ebner AD, Levan MD, Coker RF, Ritter JA. Limitations of Breakthrough Curve Analysis in Fixed-Bed Adsorption. Ind Eng Chem Res 2016. doi:10.1021/acs.iecr.6b00516.

[26] Casas N, Schell J, Blom R, Mazzotti M. MOF and UiO-67/MCM-41 adsorbents for pre-combustion CO_2 capture by PSA: Breakthrough experiments and process design. Sep Purif Technol 2013;112:34–48. doi:10.1016/j.seppur.2013.03.042.

[27] Riboldi L, Bolland O. Comprehensive analysis on the performance of an IGCC plant

with a PSA process integrated for CO_2 capture. Int J Greenh Gas Control 2015;43:57–69. doi:10.1016/j.ijggc.2015.10.006.

[28] Khurana M, Farooq S. Integrated Adsorbent-Process Optimization for Carbon Capture and Concentration Using Vacuum Swing Adsorption Cycles. AIChE J 2017;63:2987–95. doi:10.1002/aic.15602.

[29] Casas N, Schell J, Joss L, Mazzotti M. A parametric study of a PSA process for pre-combustion CO_2 capture. Sep Purif Technol 2013;104:183–92. doi:10.1016/j.seppur.2012.11.018.

[30] Khalil SH, Aroua MK, Daud WMAW. Study on the improvement of the capacity of amine-impregnated commercial activated carbon beds for CO_2 adsorbing. Chem Eng J 2012;183:15–20. doi:10.1016/j.cej.2011.12.011.

[31] Casas N, Schell J, Pini R, Mazzotti M. Fixed bed adsorption of CO_2/H_2 mixtures on activated carbon: Experiments and modeling. Adsorption 2012;18:143–61. doi:10.1007/s10450-012-9389-z.

[32] Riboldi L, Bolland O, Ngoy JM, Wagner N. Full-plant analysis of a PSA CO_2 capture unit integrated in coalfired power plants: Post- And pre-combustion scenarios. Energy Procedia 2014;63:2289–304. doi:10.1016/j.egypro.2014.11.248.

[33] Riboldi L, Bolland O. Evaluating Pressure Swing Adsorption as a CO_2 separation technique in coal-fired power plants. Int J Greenh Gas Control 2015;39:1–16. doi:10.1016/j.ijggc.2015.02.001.

[34] Dowling AW, Vetukuri SRR, Biegler LT. Large-Scale Optimization Strategies for Pressure Swing Adsorption Cycle Synthesis. AIChE J 2012;58:3777–91. doi:10.1002/aic.13928.

[35] Ribeiro AM, Grande CA, Lopes FVS, Loureiro JM, Rodrigues AE. A parametric study of layered bed PSA for hydrogen purification. Chem Eng Sci 2008;63:5258–73. doi:10.1016/j.ces.2008.07.017.

[36] Wang Y, Dowling AW, Krieft C, Walther A, Biegler LT. Pressure Swing Adsorption Optimization Strategies for CO_2 Capture. vol. 36. Elsevier; 2015. doi:10.1016/B978-0-444-63472-6.00008-2.

[37] Wakao N, Kaguei S, Funazkri T. Effect of Fluid Dispersion Coefficients Particle-to-Fluid Heat Transfer Coefficients in Packed Beds. Chem Eng Sci 1979;34:325–36. doi:0009-2509/79/0301-0325/S02 00/0.

[38] Lopes FVS, Grande CA, Ribeiro AM, Oliveira ELG, Loureiro M. Enhancing Capacity of Activated Carbons for Hydrogen Purification. Ind Eng Chem Res 2009;48:3978–90. doi:10.1021/ie801132t.

[39] Lopes FVS, Grande CA, Rodrigues AE. Activated carbon for hydrogen purification by pressure swing adsorption: Multicomponent breakthrough curves and PSA performance. Chem Eng Sci 2011;66:303–17. doi:10.1016/j.ces.2010.10.034.

[40] García S, Pis JJ, Rubiera F, Pevida C. Predicting mixed-gas adsorption equilibria on activated carbon for precombustion CO_2 capture. Langmuir 2013;29:6042–52. doi:10.1021/la4004998.

[41] Hao P, Shi Y, Li S, Zhu X, Cai N. Correlations between adsorbent characteristics and the performance of pressure swing adsorption separation process. Fuel 2018;230:9–17. doi:10.1016/j.fuel.2018.05.030.

[42] Bai BC, Kim EA, Lee CW, Lee Y-S, Im JS. Effects of surface chemical properties of activated carbon fibers modified by liquid oxidation for CO_2 adsorption. Appl Surf Sci

2015;353:158–64. doi:10.1016/j.apsusc.2015.06.046.

[43] Campbell IM. Catalysis at surfaces. 1st Ed. London, UK: Chapman and Hall Ltd; 1988.

[44] Sun N, Sun C, Liu J, Liu H, Snape CE, Li K, et al. Surface-modified spherical activated carbon materials for pre-combustion carbon dioxide capture. RSC Adv 2015;5:33681–90. doi:10.1039/C5RA02665B.

[45] Farooq S, Ruthven DM. Heat effects in adsorption column dynamics. 2. Experimental validation of the one-dimensional model. Ind Eng Chem Res 1990;29:1084–90. doi:10.1021/ie00102a020.

[46] Wang Y, Dowling AW, Krieft C, Walther A, Biegler LT. Pressure Swing Adsorption Optimization Strategies for CO_2 Capture. Comput Aided Chem Eng 2015;36:197–223. doi:10.1016/B978-0-444-63472-6.00008-2.

List of Figure Captions.

Figure 1. Schematic figure of the fixed-bed reactor process using Pressure Swing Adsorption (PSA) at laboratory scale.

Figure 2. Experimental breakthrough curves for the adsorption step of PSA using AC-Unmodified and AC-MEA-MDEA.

Figure 3. Comparison of the dispersed plug flow model against experimental data using glass beads under PSA conditions.

Figure 4a. Parameter estimation between the model and the experimental data for 30% and 40% CO_2 feed fractions using AC-MEA-MDEA.

Figure 4b. Parameter estimation between the model and the experimental data for 30% and 40% CO_2 feed fractions using AC-TEPA.

Figure 5. Schematic figure of the steps undertaken in the PSA process.

Figure 6. The effect of the mass transfer coefficient (K) on the outlet molar fractions of CO_2 for a seven-step PSA process.

Figure 7. The effect of feed pressure (P_{feed}) on the outlet molar fractions of CO_2 for a seven-step PSA process.

Figure 8. The effect of feed molar fractions (Y_{feed}) on the outlet molar fractions of CO_2 for a seven-step PSA process.

Figure 1

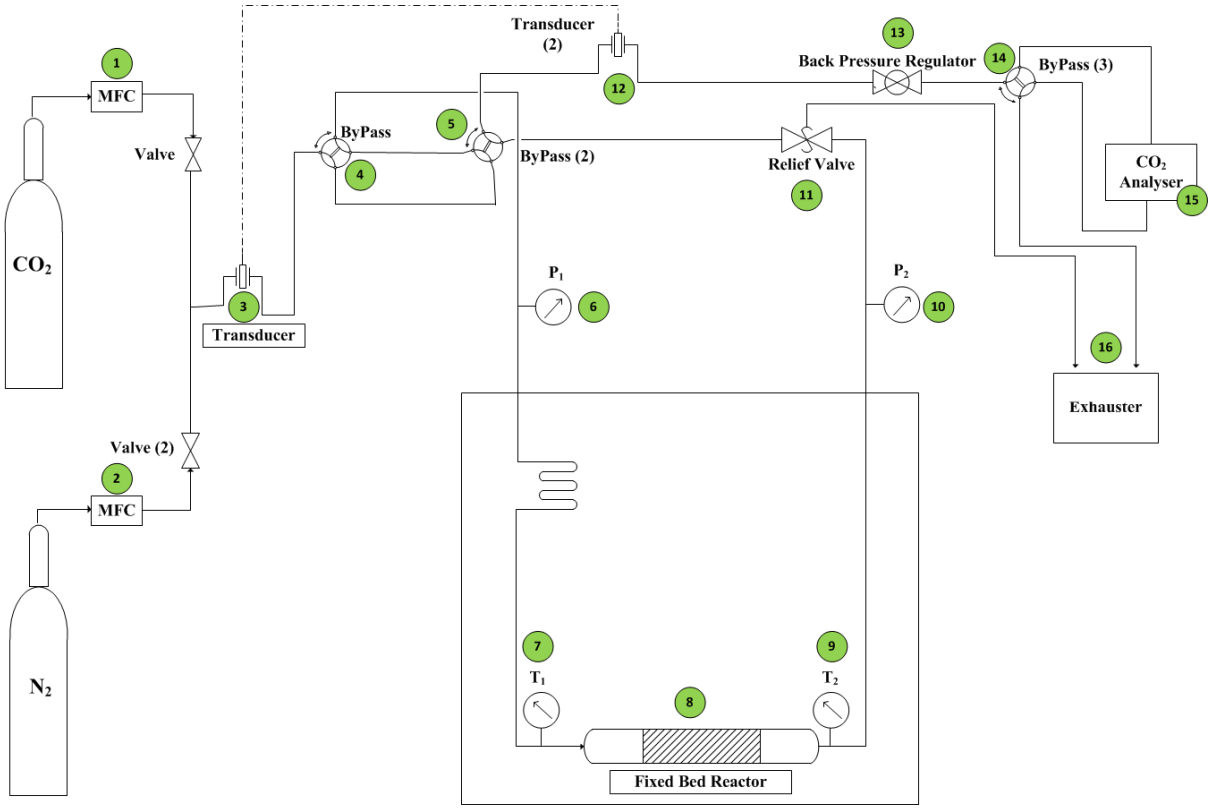

Figure 2

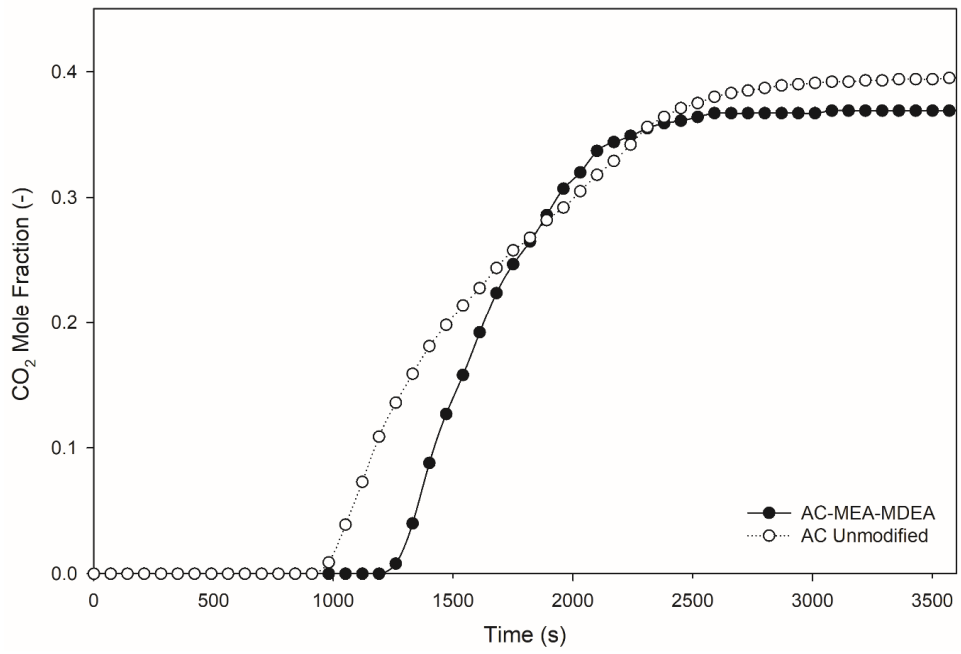

Figure 3

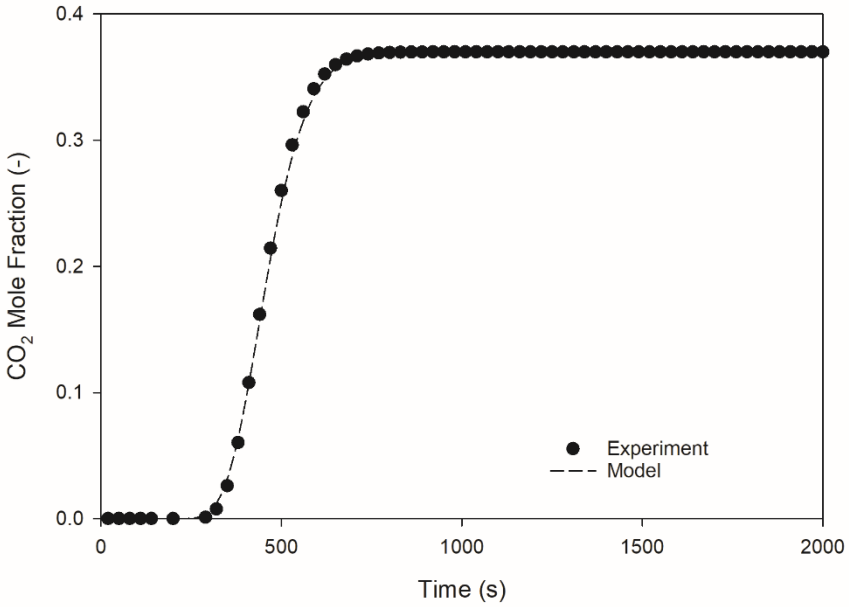

Figure 4a

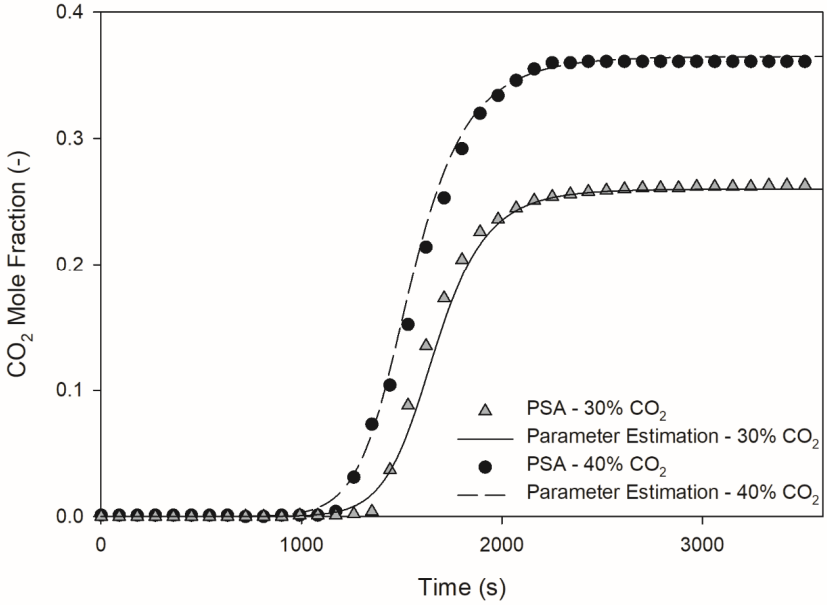

Figure 4b

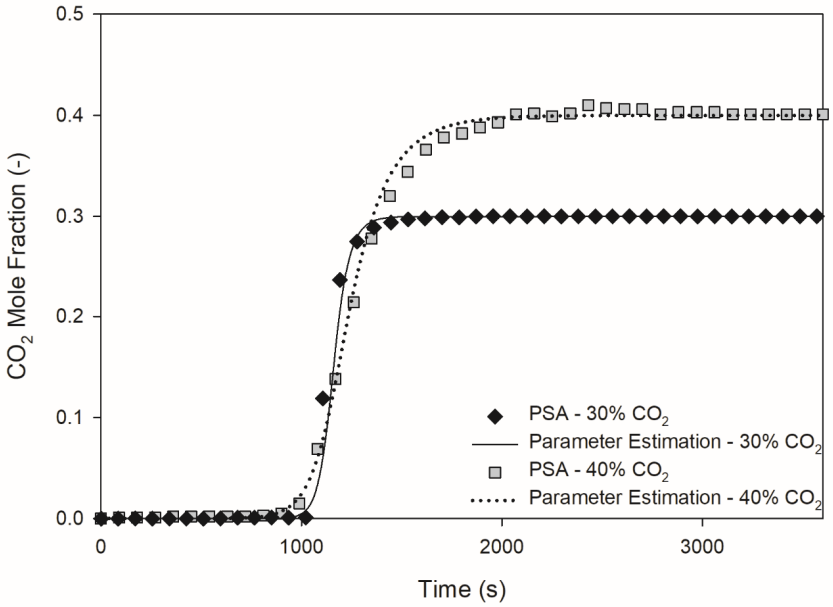

Figure 5

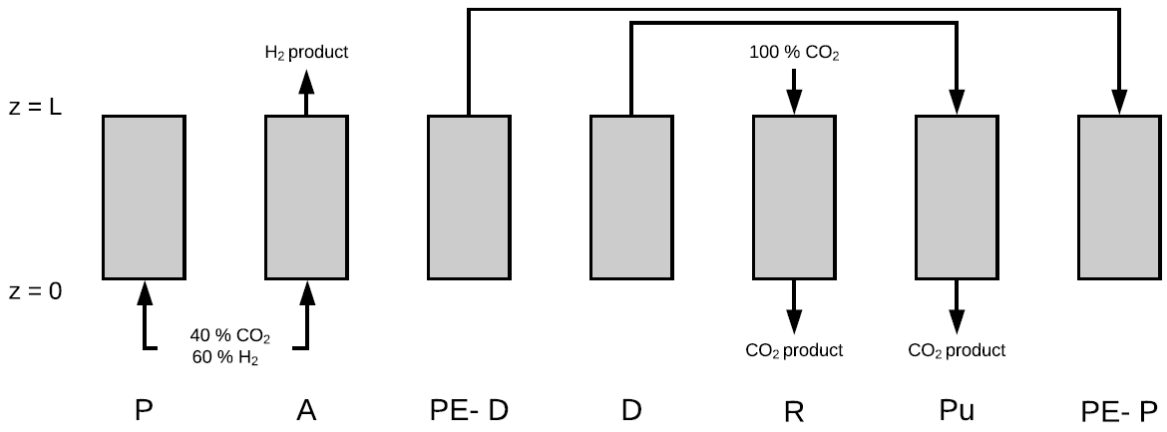

Figure 6

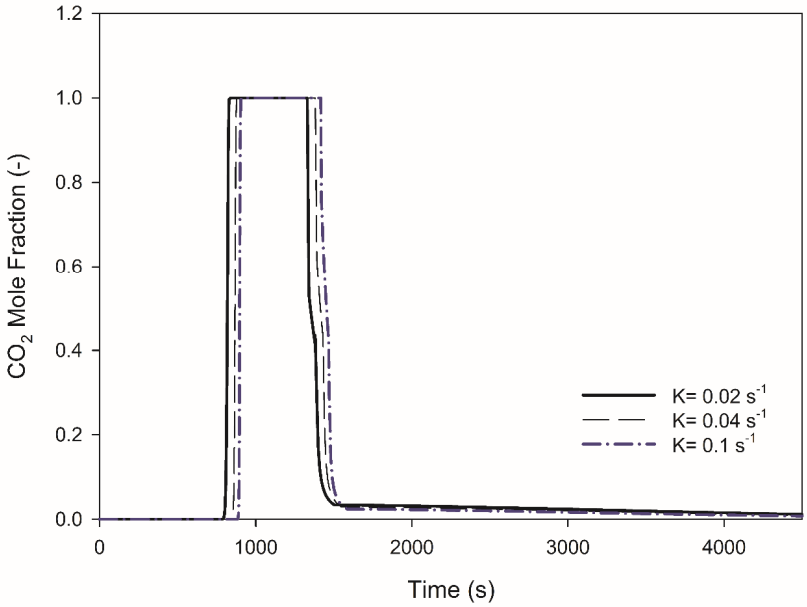

Figure 7

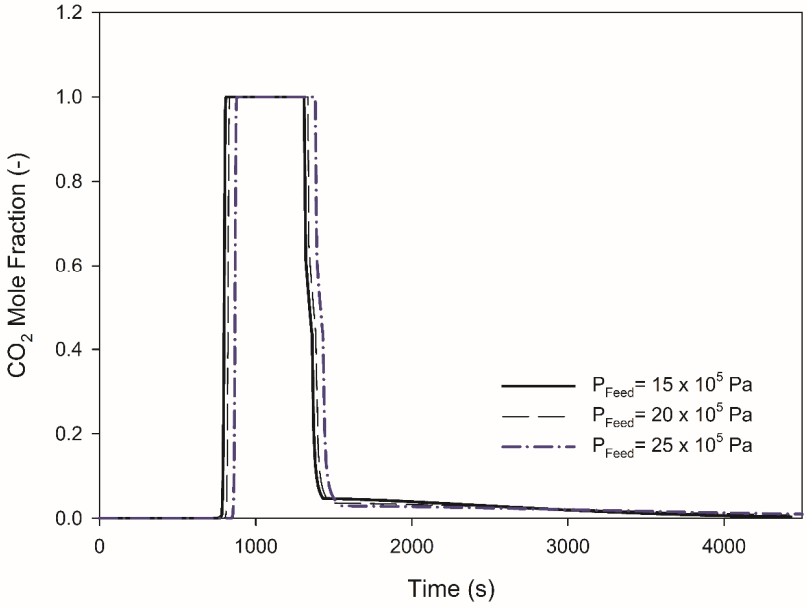

Figure 8

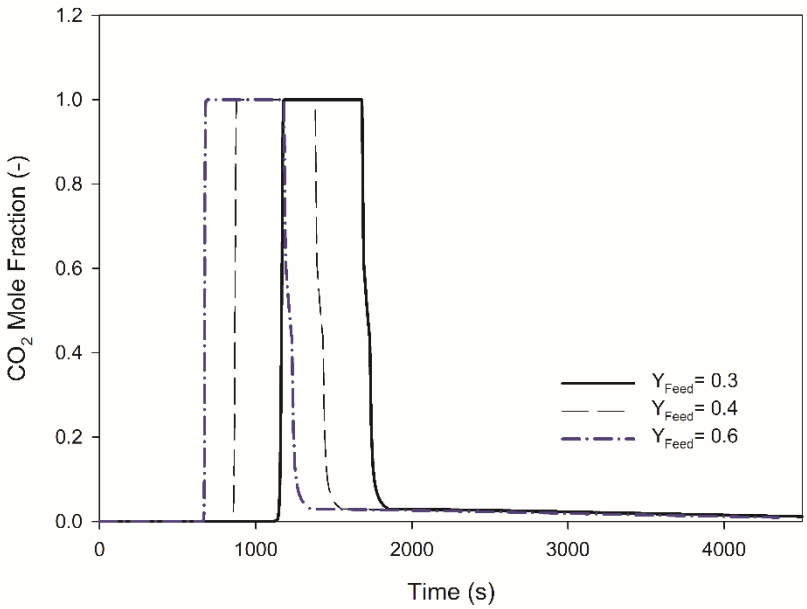
1.2
1.0
0.8
0.6
0.4
0.2
0.0
CO_2 Mole Fraction (-)
0
1000
2000
3000
4000
Time (s)
Y_{Feed}= 0.3
Y_{Feed}= 0.4
Y_{Feed}= 0.6